Combining NIR Transmission Spectroscopy, Time-Resolved Spectroscopy and Diffusion Theory for Analysis of Intact Pharmaceutical Tablets

Birgitta Strömdahl
Alexandra Löwgren

Master's Thesis

Lund Reports on Atomic Physics, LRAP-334
Lund, November 2004

Abstract

In recent years Near Infrared (NIR) Spectroscopy has become a valuable technique for determining the amount of active substance in pharmaceutical tablets. This is due to its fast and non-destructive performance. Even though this method works well it suffers from a few drawbacks, which makes improvements of interest. Conventional NIR spectroscopy is unable to separate the scattering from the absorption, whereas this is possible with time-resolved spectroscopy. In this thesis, two different evaluation methods were used to extract the absorption coefficients from the scattering coefficients in the conventional NIR measurements by using time-resolved spectroscopy and diffusion theory. These methods eliminated the effects of scattering and reconstructed the true absorption. Chemometric evaluations showed that both evaluation methods investigated in this thesis were better than conventional NIR spectroscopy to predict the amount of active substance. Not only was the chemical content analyzed, but also other tablet features. It appeared as if the particles in the tablets were lumped together during manufacturing when the compression force reached a certain limit. It was also seen that the scattering decreased with increasing concentration of active substance due to the reduced amount of microcrystalline cellulose. The two evaluation methods also appeared very robust. They were for example able to predict tablets with physical features differing from the ones used in the calibration set.

Table of Contents

1. Introduction

The requirements on the pharmaceutical companies to determine the amount of active substance, with high precision, calls for the development of new techniques. In recent years Near Infrared (NIR) Spectroscopy has become a valuable technique for determining the amount of active substance in pharmaceutical tablets. The advantages of this method are that it is non-destructive, fast and can be remotely performed. However, the method suffers from some drawbacks. It needs frequent recalibrations and it is not very robust.

The amount of active substance is determined based on Beer-Lamberts law, which describes the attenuation as a function of absorption. This law is not valid in turbid media, such as a pharmaceutical tablet, since the attenuation of light when it passes through the tablet depends not only on absorption but also on scattering. The scattering is highly affected by physical properties such as thickness, particle size and shape. Differences in these properties therefore strongly influence the conventional NIR spectrum, but it is impossible to distinguish whether the attenuation depends on scattering or absorption. Hence, a variation in light scattering can affect the evaluation of content of active substance leading to erroneous results.

Methods to separate scattering and absorption are available. By using time-resolved spectroscopy, frequency-resolved spectroscopy or spatially-resolved spectroscopy, this separation can be achieved. In this thesis the method of interest is time-resolved spectroscopy. The system used performs time-resolved measurements in a broad wavelength region. The drawbacks of this method are that the instrumentation is expensive and the experimental setup needs time consuming alignments. A less expensive and faster system could be constructed if the measurements could be made for just a few discrete wavelengths. This can be done by using diode lasers or by scanning a tunable laser over the wavelength regions of interest. In this thesis such a system is simulated in the evaluations by extracting information from a few selected wavelength regions instead of using the entire time-resolved wavelength region.

The outline of this project is to enhance the performance of the conventional NIR measurements by means of time-resolved spectroscopy. While conventional NIR spectroscopy is a steady-state method which only gives the absorbance, time-resolved spectroscopy gives information about when and how much of the light that is transmitted. By means of diffusion theory and the time-resolved measurements a correction of conventional NIR data is performed. This correction eliminates the effects of scattering and reconstructs the true absorption. To validate the performance of the correction, multivariate analysis as well as reference analysis is made.

2. Theory

2.1. Light Interaction with Media

Light that falls on the surface of a solid material will partly be reflected. The amount of light that is reflected is strongly dependent on the angle of incidence. The light that is transmitted through the surface is thereafter scattered around in the medium until it is either absorbed or transmitted out of the boundary of the medium in an arbitrary direction. [1]

If the energy of the light that travels through the medium corresponds to the difference between two energy levels in a molecule or atom, the light can be absorbed. Thus the absorption is strongly dependent on the wavelength of the light. Since the energy levels are unique for each type of molecule or atom, the absorption spectrum is like a fingerprint. The absorption can therefore be a valuable instrument to determine the contents of molecules or atoms in a medium. [1] In the near infrared region the absorptions are due to vibrational overtone transitions and combination bands. [6]

The scattering in a medium can be either elastic or inelastic. Elastic scattering means that the energy of light is conserved whereas the inelastic scattering involves energy changes. There are two types of elastic scattering, Rayleigh and Mie. If the particle size is less than the wavelength of light, the light is Rayleigh scattered. Mie scattering occurs when the particles are much greater than the wavelength. Both Rayleigh and Mie scattering are strongly wavelength dependent. Rayleigh scattering depends on wavelength according to λ^{-4}. The Mie scattering dependence on wavelength is far more complicated and depends on for instance particle size, shape and refractive index. The Mie scattering dependence can be approximated by λ^{-b}, where $b \leq 2$. An example of inelastic scattering is the Raman effect with the down- and upshifted components from the Rayleigh frequency, the Stokes and Anti-Stokes lines. [6][9]

2.2. Transport Theory

Light can be described as both travelling waves and particles. When seen as waves the light is described by Maxwell's equations. How much of the light that will be absorbed, scattered and transmitted depends on the optical properties of the material. These phenomena are complicated to describe with Maxwell's equations. If light is instead considered as a stream of particles, photons, the light distribution in the medium can be described by transport theory. This theory describes the optical properties absorption and scattering by means of the absorption coefficient and the scattering coefficient respectively. There is also a scattering phase function which relates to the probability of scattering in different directions. [2] Transport theory is, for example, applicable in problems considering heat conduction, diffusion, neutrons in nuclear reactions and light propagation in turbid media [3].

When observing light propagation it is important to consider the conservation of energy. The flow of photons in a direction $\boldsymbol{s}$ in a small volume dV is described in Figure 2.1.

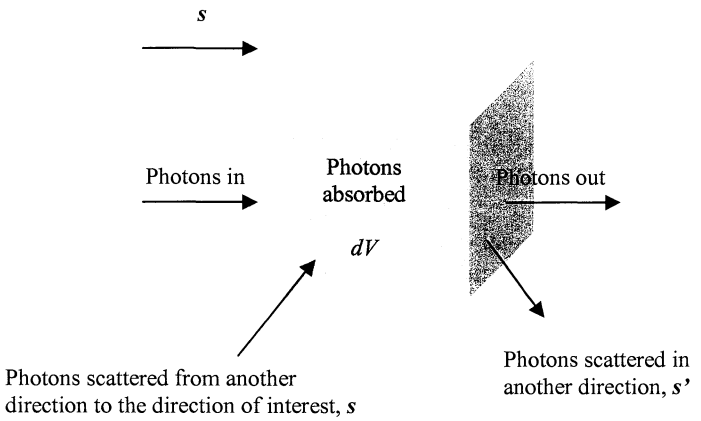

Figure 2.1
The flow of photons in an infinitesimal volume dV.

The photon density function, $N(\mathbf{r},\mathbf{s},t)$, is the number of photons with the direction $\mathbf{s}$ at time t per volume unit and solid angle. This function is used to describe the flow of photons with time according to Eqn. 2.1, where $\mathbf{r}$ is the coordinates of the volume element, and $\mathbf{s}$ is the direction of photons at time t.

Eqn. 2.1

$$\int_V \frac{\partial N(\mathbf{r},\mathbf{s},t)}{\partial t} dV$$

This expression describes the changes in the photon distribution over time. The changes are due to boundary losses, scattering in another direction $\mathbf{s}'$, absorption, photons gained from another direction $\mathbf{s}'$ into direction $\mathbf{s}$ and photons gained through a light source, q. These contributions add up to the transport equation (Eqn. 2.2).

Eqn. 2.2

$$\int_V \frac{\partial N(\mathbf{r},\mathbf{s},t)}{\partial t} dV = -\int_V c\mathbf{s}\cdot\nabla N(\mathbf{r},\mathbf{s},t)dV - \int_V c\mu_s(\mathbf{r})N(\mathbf{r},\mathbf{s},t)dV - \int_V c\mu_a(\mathbf{r})N(\mathbf{r},\mathbf{s},t)dV + \\ + \int_V c\mu_s(\mathbf{r})\int_{4\pi} p(\mathbf{s}',\mathbf{s})N(\mathbf{r},\mathbf{s}',t)d\omega' dV + \int_V q(\mathbf{r},\mathbf{s},t)dV$$

In this expression $p(\mathbf{s},\mathbf{s}')$ is the phase function, which gives the probability for scattering from $\mathbf{s}$ to $\mathbf{s}'$, and c is the velocity of light in the medium. The above mentioned absorption and scattering coefficients are given by μ_a and μ_s. μ_a and μ_s is defined as the probability for absorption and scattering per unit length. [3] In turbid media the phase function can be approximated by the Henyey-Greenstein phase function (Eqn. 2.3), where g is given by Eqn. 2.4.

Eqn. 2.3

$$p(\cos\theta) = \frac{1}{4\pi}\frac{1-g^2}{\left(1+g^2-2g\cos\theta\right)^{3/2}}$$

Eqn. 2.4

$$g = \langle \cos\theta \rangle$$

g is the anisotropy factor and describes how the photons are directed after scattering (Figure 2.2). If g equals 1, all photons are scattered in the forward direction and total backscattering is represented by g equals -1. For g equals 0 photons are in average scattered equally forward and backwards, so called isotropic scattering. When g is not equal to zero another type of scattering coefficient could be used, the reduced scattering coefficient. The definition of the reduced scattering coefficient is given by Eqn. 2.5. The inverse of μ_s' is a measure of the average distance a photon travels before the scattering can be regarded as isotropic. μ_s' is therefore used to assume isotropic scattering, although this is not the case. Hereafter only the reduced scattering coefficient will be used, and it will therefore be referred to as the scattering coefficient. [1][2]

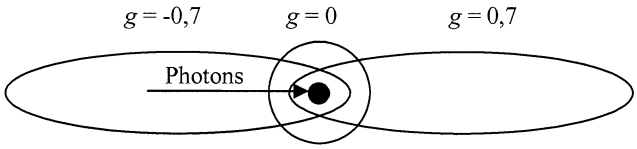

Figure 2.2
The Henyey-Greenstein phase function for three different values of g.

Eqn. 2.5

$$\mu_s' = (1-g)\mu_s$$

Under the simplification that the scatterers are spherical and independent, the scattering coefficient is wavelength dependent according to Mie theory, see Eqn. 2.6. [9]

Eqn. 2.6

$$\mu_s' = a\lambda^b$$

It is also common to express the transport equation by means of radiance $L(\mathbf{r},\mathbf{s},t)$ in $[Wm^{-2}sr^{-1}]$. This leads to Eqn. 2.7. [3]

Eqn. 2.7

$$\frac{1}{c}\frac{\partial L(\mathbf{r},\mathbf{s},t)}{\partial t} = -\mathbf{s}\cdot\nabla L(\mathbf{r},\mathbf{s},t) - (\mu_s + \mu_a)L(\mathbf{r},\mathbf{s},t) + \mu_s \int_{4\pi} L(\mathbf{r},\mathbf{s}',t)p(\mathbf{s},\mathbf{s}')d\omega' + q(\mathbf{r},\mathbf{s},t)$$

2.3. Diffusion Approximation

The transport equation can be solved analytically or numerically. However, the expression is rather complex, and therefore simplifications are necessary. Solutions to transport theory can be obtained by for example the Monte Carlo method, the Adding-Doubling method or the diffusion approximation. Here only the diffusion approximation will be described.

Light is diffuse when it fulfils the following criteria; the scattering must be nearly isotropic, the reduced scattering coefficient must be much larger than the absorption coefficient, and the photon flow must be calculated far away from the light source, that is more than ten scattering events from the source. If the scattering would not be isotropic, the light would be pointed in a certain direction. A high absorption would prevent the light from being diffuse since not enough scattering events would occur before the light is absorbed. Similarly the photon flow must be calculated far away from the source so that a sufficient amount of scattering events will occur and give rise to diffuse light. Diffuse light implies a spherical symmetry, and therefore the radiance L can be expanded in spherical harmonics according to Eqn. 2.8. Furthermore, based on the criteria above, two approximations can be made. The light source is assumed to be isotropic, and the flux vector, $\boldsymbol{J}$ [W/m^2], is assumed to be constant in time. These approximations lead up to the diffusion equation (Eqn. 2.9), where the diffusion coefficient D is given by Eqn. 2.10. [2]

Eqn. 2.8

$$L(\mathbf{r},\mathbf{s},t)=\sum_{l=0}^{\infty}\sum_{m=-l}^{l}\sqrt{\frac{2l+1}{4\pi}}L_{lm}(\mathbf{r},t)Y_{lm}(\mathbf{s})$$

Eqn. 2.9

$$\frac{1}{c}\frac{\partial\phi(\mathbf{r},t)}{\partial t}=\nabla D(\mathbf{r})\nabla\phi(\mathbf{r},t)-\mu_a\phi(\mathbf{r},t)+q(\mathbf{r},t)$$

Eqn. 2.10

$$D=\frac{1}{3(\mu_a+\mu_s')}$$

2.3.1. Transmission

The diffusion equation can be solved analytically by means of Green's functions. In case of a pencil beam illuminating a sample with an infinite slab geometry, an approximation is made by introducing a point source in the medium at a distance z_0, equal to the inverse of μ_s', from the surface where z = 0 (Figure 2.3). This is also applicable for many types of simple geometries as long as the solutions are calculated for points far away from the source. If the refractive indices of the sample and the surrounding media are matched, the fluence rate equals zero at the boundaries. Since the indices usually differ, reflections will occur, and hence extrapolated boundaries, where the fluence rate equals zero, must be introduced at a distance z_e from the surfaces (Eqn. 2.11). Here n equals the refractive index of the medium. [2][3]

Eqn. 2.11

$$z_e=2AD=2\frac{1+r_d}{1-r_d}D,$$

$$\text{where}\quad r_d=-\frac{1.440}{n^2}+\frac{0.71}{n}+0.668+0.0636\cdot n$$

Mirror sources are introduced around the extrapolated boundaries to fulfil the boundary condition. This is illustrated in Figure 2.3. The more mirror sources that are used, the better the result. For the case of a homogeneous slab with thickness d, the time-resolved fluence rate is given by Eqn. 2.12. [2][4]

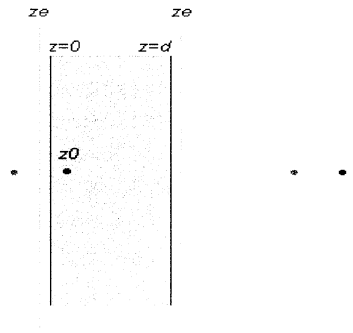

Figure 2.3
A few mirror sources for a slab with extrapolated boundaries at both surfaces. The darker dots illustrate positive sources while the brighter dots illustrate negative sources.

Eqn. 2.12

$$\phi(r,z,t)=\frac{c}{(4\pi Dct)^{3/2}}\exp\left(-\mu_a ct-\frac{r^2}{4Dct}\right)\left\{\sum_{m=-\infty}^{\infty}\exp\left[-\frac{(z-z_{+,m})^2}{4Dct}\right]-\right.$$

$$\left.-\sum_{m=-\infty}^{\infty}\exp\left[-\frac{(z-z_{-,m})^2}{4Dct}\right]\right\},\quad \text{where}$$

$$z_{+,m}=2m(d+2z_e)+z_0 \quad \text{for positive sources,}$$

$$z_{-,m}=2m(d+2z_e)-2z_e-z_0 \quad \text{for negative sources.}$$

The time-resolved transmission is given by the photon current leaving the slab at $z=d$ and is described by Eqn. 2.13.

Eqn. 2.13

$$T(r,t)=-D\hat{\mathbf{n}}\cdot\nabla\phi(r,z,t)\big|_{z=d}=-D\frac{\partial\phi}{\partial z}\bigg|_{z=d}$$

Inserting the time-resolved fluence rate, Eqn. 2.12, into the expression for the time-resolved transmission, Eqn. 2.13, yields the transmission for a slab, Eqn 2.14.

Eqn. 2.14

$$T(r,t)=\frac{\exp\left(-\mu_a ct-\frac{r^2}{4Dct}\right)}{2(4\pi Dc)^{3/2}t^{5/2}}\sum_{m=-\infty}^{\infty}\left[z_{1,m}\exp\left(-\frac{z_{1,m}^2}{4Dct}\right)-z_{2,m}\exp\left(-\frac{z_{2,m}^2}{4Dct}\right)\right],\quad \text{where}$$

$z_{1,m}=d(1-2m)-4mz_e-z_0$ for positive sources,

$z_{2,m}=d(1-2m)-(4m-2)z_e+z_0$ for negative sources.

To get the steady-state expression for the transmission, the time-resolved expression, Eqn 2.14 is integrated over time, and Eqn. 2.15 is obtained.

Eqn. 2.15

$$T(r)=\frac{1}{4\pi}\sum_{m=-\infty}^{\infty}\left(z_{1,m}\left(r^2+z_{1,m}^2\right)^{-3/2}\left\{1+\left[\frac{\mu_a\left(r^2+z_{1,m}^2\right)}{D}\right]^{1/2}\right\}\exp\left\{-\left[\frac{\mu_a\left(r^2+z_{1,m}^2\right)}{D}\right]^{1/2}\right\}-\right.$$

$$\left.-z_{2,m}\left(r^2+z_{2,m}^2\right)^{-3/2}\left\{1+\left[\frac{\mu_a\left(r^2+z_{2,m}^2\right)}{D}\right]^{1/2}\right\}\exp\left\{-\left[\frac{\mu_a\left(r^2+z_{2,m}^2\right)}{D}\right]^{1/2}\right\}\right)$$

2.4. Time-Resolved Spectroscopy

Time-resolved measurements are performed by illuminating the medium of interest with a short laser pulse, in the femto- or picosecond regime. The transmitted or reflected light is then recorded as a function of time. If the conditions for the diffusion approximation are fulfilled the optical properties can be derived from the shape of the measured time-dispersion curve. The optical properties can be found by fitting the measured time-resolved curve to the analytical expression of the diffusion equation, with respect to the absorption and scattering coefficients. This can be done by using a non-linear curve-fitting algorithm, for example the Levenberg-Marquardt Method, as described in section 2.6.

2.5. Near Infrared Transmission Spectroscopy

Near infrared measurements are performed by illuminating the sample with a steady-state light source in the near infrared wavelength region. The transmitted light, I, is measured together with the intensity of the light from the source, I_o. The result is given as absorbance, which is defined in Eqn. 2.16.

Eqn. 2.16

$$A=\log^{10}\left(\frac{I_0}{I}\right),\ \text{where}\ \frac{I}{I_0}\ \text{is the transmission.}$$

2.6. Levenberg-Marquardt Method

Assume that (x_i,y_i) are measured data which are described by the model $y=y(x,\boldsymbol{p})$, where $\boldsymbol{p}$ are the desired parameters from measurements. The merit function is then defined as Eqn. 2.17, where σ_i usually estimates the standard deviation. [3]

Eqn. 2.17

$$\chi^2(\mathbf{p}) = \sum_{i=1}^{N} \left(\frac{y_i - y(x_i, \mathbf{p})}{\sigma_i} \right)^2$$

By means of the Levenberg-Marquardt Method, which is a type of Steepest Descent Method, the merit function can be minimized. The Steepest Descent Method finds the minimum by walking down the gradient. If the initial guess is $\boldsymbol{p_k}$, the next step is given by Eqn. 2.18. [3]

Eqn. 2.18

$$\mathbf{p}_{k+1} = \mathbf{p}_k - C \cdot \nabla \chi^2, \quad \text{where } C > 0 \text{ is the stepsize}$$

The gradient has information about the slope in one point, but no information about how long it will remain constant. This makes it difficult to determine the step size, *C*, and the convergence is therefore uncertain. When the initial guess is close to the minimum, it is better to use the Inverse Hessian Method that uses the second derivative of the merit function to find the minimum. The Levenberg-Marquardt Method combines the Steepest Descent Method and the Inverse Hessian Method to minimize the merit function regardless of the distance between the initial guess and the minimum. [3]

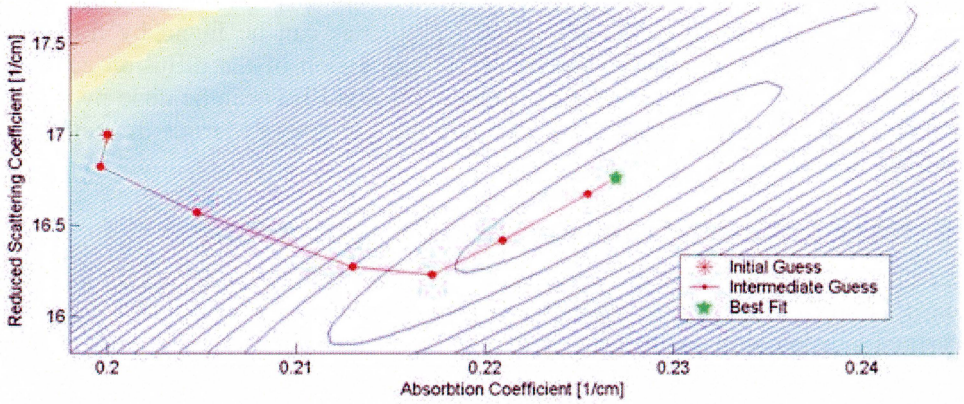

Figure 2.4
Levenberg-Marquardt algorithm. The elliptical curves are equidistant isocurves to the function one wishes to minimize.

2.7. Multivariate Analysis

Most chemical measurements are rather complex, meaning that they depend on many parameters. The method to relate measurements made on a chemical system to the states of the system by means of applications of mathematical or statistical methods is

called chemometrics. Due to the simultaneous dependency on multiple variables, chemometrics is often labelled as multivariate analysis. The fundamental task is to find relations between the variables. This can be done by Principal Component Analysis (PCA). Further, the sample measurements can be evaluated in relation to a reference analysis by Partial Least Squares (PLS) Regression. [7]

2.7.1. PCA

The basis for PCA is to find a set of axes, called principal components, along which the data set has the strongest covariance. By graphically illustrating the data along two principal components, groupings, trends and outliers in the data can be observed. [8]
The aim of finding principal components is that the data can be described with fewer factors than the original variables. However, there will always be a residual matrix, but the number of principal components is chosen so that most of the information in the data matrix will be included in the system of principle components. The residual matrix will then only describe variations due to noise. Hence, this is a way to find a simplified model of the data. [7]

Briefly, the principal components are found by assuming that $\boldsymbol{X}$ is a data matrix with m rows and n columns, where columns represent variables and rows represent samples. Then, by means of PCA, $\boldsymbol{X}$ can be expressed as the sum of the inner product of vectors $\boldsymbol{t}_i$ and $\boldsymbol{p}_i$ plus a residual matrix $\boldsymbol{E}$ (Eqn. 2.19). [7]

Eqn. 2.19

$$\mathbf{X} = \mathbf{t}_1\mathbf{p}_1^T + \mathbf{t}_2\mathbf{p}_2^T + \ldots + \mathbf{t}_k\mathbf{p}_k^T + \mathbf{E}, \text{ where } k \leq \min(m,n).$$

The $\boldsymbol{t}_i$ vectors are called scores and describe the relations between the samples. The $\boldsymbol{p}_i$ vectors on the other hand describe the relations between the variables, and they are known as loadings. The $\boldsymbol{p}_i$ vectors are eigenvectors of the covariance matrix as given by Eqn. 2.20, and the covariance matrix is defined in Eqn. 2.21.This definition is valid when the columns of matrix $\boldsymbol{X}$ have been mean centred, which means that the original mean have been subtracted from each column to give a zero mean.[7]

Eqn. 2.20

$$\mathrm{cov}(\mathbf{X})\mathbf{p}_i = \lambda_i \mathbf{p}_i$$

Eqn. 2.21

$$\mathrm{cov}(\mathbf{X}) = \frac{\mathbf{X}^T\mathbf{X}}{m-1}$$

The score vector $\boldsymbol{t}_i$ is a linear combination of the matrix $\boldsymbol{X}$ and $\boldsymbol{p}_i$ (Eqn. 2.22).

Eqn. 2.22

$$\mathbf{X}\mathbf{p}_i = \mathbf{t}_i$$

2.7.2. PLS

PLS is a method to find the best solution to a matrix equation. The big difference to PCA is that it is not only to find suitable principal components to the data matrix, but

simultaneously find a good correlation with y data. The y data is a vector of reference measurements for each sample, for instance the amount of active substance in a pharmaceutical tablet. [8]

By using a selected part of the $\boldsymbol{X}$ matrix and the corresponding part of the $\boldsymbol{y}$ vector a model is created. This model is then used to predict the y values corresponding to another part of the $\boldsymbol{X}$ matrix. The values used to create the model are called calibration set, and the values that are predicted with the model are called validation set. If the agreement between the reference measurements and the predicted values is good, the model can be considered as a good system and can thereafter be used to predict new samples without reference measurements. [7]

A measure of how correct the predictions are is the Root Mean Square Error of Prediction (RMSEP). This is defined in Eqn. 2.23, where $\hat{y}_i$ are the predicted variables while y_i are the values of the $\boldsymbol{y}$ vector and n is the number of samples predicted. The RMSEP value is often divided by the mean value of the $\boldsymbol{y}$ vector to obtain the percentage of RMSEP. [7]

Eqn. 2.23

$$RMSEP = \sqrt{\frac{\sum_{i=1}^{n}(\hat{y}_i - y_i)^2}{n}}$$

3. Material and Methods

3.1. Sample Description

The samples were tablets produced in a cylindrical shape with flat end surfaces, a diameter of 10 *mm* and a thickness varied between 1.85-2.75 *mm*. All tablets had the same weight. By varying the compression force during the manufacturing process, the different thicknesses of the tablets were obtained. The tablets were compressed with a compression force around 3 *kN*. Three different types of granulates were used to produce the tablets: G1, G10 and G17. Each granulate contained different amounts of active substance: G1 had the lowest amount of active substance and G17 the highest. The granulate was filtered so that each tablet contained particles less than 150 μm, between 150-400 μm, or greater than 400 μm. The population investigated consisted of 82 tablets with approximately 9 tablets of each combination of particle size and granulate.

Since the particle sizes greatly exceed the NIR wavelengths used in this thesis, the light scattering will be treated according to Mie theory. Due to the high scattering and low absorption in the tablets they can be considered as turbid media, and therefore the diffusion equation is applicable. The high number of scattering events in the tablets implies that the diameter can be considered infinite, and therefore the tablet can be approximated as a slab as in Figure 2.3.

3.2. Time-Resolved Measurements

3.2.1. System Description

In the time-resolved measurements an Ar-ion laser pumped mode-locked Ti:Sapphire laser was used. The pulse length from the laser was shorter than 100 *fs* with an energy of 4 *nJ*. The repetition rate of the laser was 80 *MHz*, and the wavelength was centred around 800 *nm*. The laboratory setup is illustrated in the left part of Figure 3.1. The right part of the figure shows an image of a sample measurement recorded by the streak camera. The image shows that the measurements are both spectrally as well as time resolved.

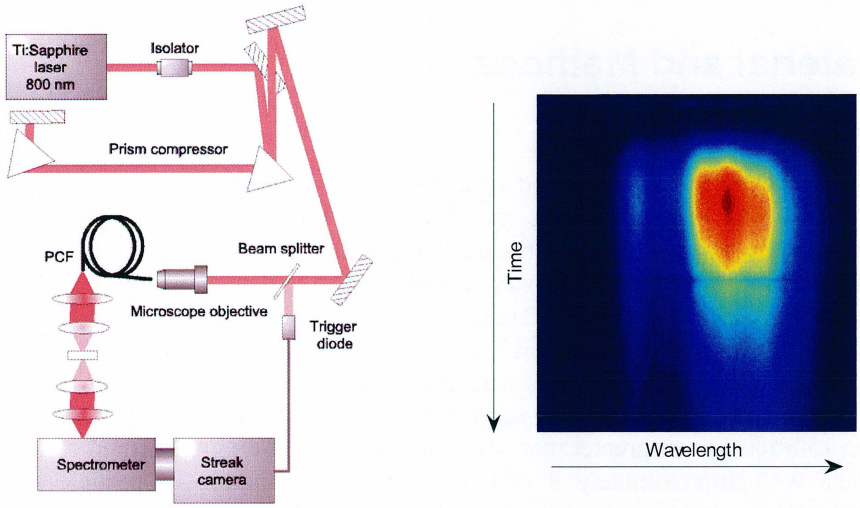

Figure 3.1
Left: Laboratory setup for time-resolved measurements.
Right: Image of a sample measurement versus time and wavelength.

An optical isolator was used to prevent reflections back to the laser. Such reflections could influence the performance of the laser. Due to time dispersion caused by the optical components a prism compressor was used to achieve the shortest pulse length possible after the microscope objective. The light was focused by an x40 microscope objective lens with a numeric aperture of 0.65 into a 100 *cm* long index-guiding crystal fibre (ICF) (Crystal Fibre A/S, Copenhagen, Denmark). The core diameter of the fibre was 2 μm, and it had a minimum dispersion at 760 *nm*. The light was kept confined within the fibre for the entire length, and this resulted in nonlinear effects which broadened the light spectrum into a continuum from at least 750 to 1150 *nm*. This is seen in Figure 3.2, which is a spectrum of the instrumental response function. This function is the instruments response to a short light pulse. The instrumental response function was measured to have a FWHM of 13-14 *ps*. The pulse is broadened by the slits in the spectrometer and the streak camera as well as the grating in the spectrometer. The pulse width is also influenced by noise in the triggering of the streak camera. The light intensity was not the same throughout the entire wavelength range. However, the evaluation techniques are independent of such variations as long as the signal is detectable regarding the signal-to-noise level. This independency is due to the fact that only the shape of the time dispersion curve determines the optical properties. [5]

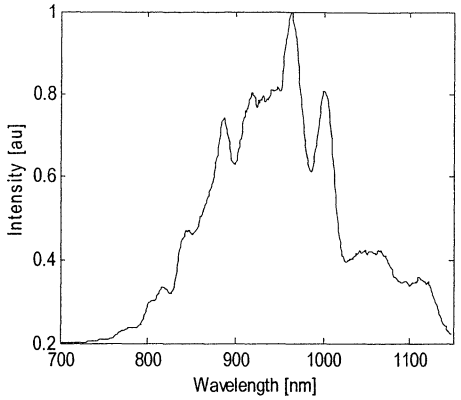

Figure 3.2
The instrumental response function versus wavelength.

After passing through the fibre the light was attenuated by a gradient neutral density filter wheel and then focused by a lens system onto the pharmaceutical tablet, which was held by an iris holder to prevent stray light from entering the spectrometer. The spot size on the tablet was approximately 2 *mm*. The diffusely transmitted light was imaged on the entrance slit of the spectrometer (Chromex, Model 250 IS) by two achromatic lenses. At the entrance an attenuation filter could be placed during the measurements. The spectrometer was equipped with a 30 *grooves/mm* grating. The light was spectrally dispersed horizontally by the spectrometer and was thereafter detected by the streak camera (Hamamatsu, Model C5680). The streak camera was trigged by a trigger diode. A streak camera works as follows: After entering the streak camera, the light impinges on a photocathode, which transforms the photons into electrons. The electrons are thereafter accelerated and focused by the use of an anode to enter between two deflection plates. A rapidly rising voltage over the plates causes vertical deflection that gives the time resolution. The electrons then pass through an adjustable Micro Channel Plate (MCP), where the electron beam is intensified. The electrons hit a phosphor plate emitting light onto a CCD-camera, from which the recorded image is transferred to the computer for further evaluations. [5][6]

3.2.2. Measurement Procedure

Before commencing the measurements it is important that the laser and the streak camera are not drifting but are stable. This takes about two hours after turning them on. The system was aligned, by means of an XYZ translation mount, so that the maximum amount of light entered the fibre. This resulted in a wavelength range that was as broad as possible, and the light exiting the fibre appeared bright green.

To increase the signal-to-noise ratio, all measurements were integrated 100 times, and the mean value of the measurements was calculated. An instrumental response function was measured for each sample, where the streak camera was set to integrate over 111 *ms*, which leads to a total integration time of 11.1 *s*. The filter in front of the spectrometer as well as the gradient filter wheel was used to maximize the signal-to-noise ratio but also to prevent damage on the streak camera. A pharmaceutical tablet was then placed in the iris holder, and measurements were performed with a longer integration time, 5004 *ms*, which lead to a total integration time of 8.3 *min*. The

gradient filter wheel was adjusted, and the filter in front of the spectrometer was removed. For each MCP setting used, a background measurement was made by blocking the laser light. The background was then subtracted from the tablet measurement. For each sample the same MCP settings was used for background, instrumental response function as well as tablet measurement to keep the dark current level constant. The slit widths of the streak camera and the spectrometer were fixed at 50 and 250 μm, respectively.

3.3. Near Infrared Transmission Measurements

The conventional NIR measurements were made with an FT-IR spectrometer (ABB Bomem, Model MB 160 PH). The FT-IR spectrometer uses a Fourier transform to separate the different frequencies of the light. The spectrometer is based on a Michelson interferometer, which consists of a fixed mirror, a moving mirror and a beamsplitter. The light that enters the interferometer is divided by the beamsplitter into two parts, where one part is aimed at the fixed mirror and the other at the moving mirror. When the moving mirror is scanned, the two light beams will interfere when reflected back to the beamsplitter with alternating constructive and destructive interference. The light then passes through the sample, and the transmitted light is recorded by a detector. The detected interferogram is Fourier transformed which yields the spectral information of the transmitted light.

The measurements were performed with an InGaAs detector with resolution 16 cm^{-1} and 32 *scans/sample* for wavelengths between 0-15000 cm^{-1}. The signal-to-noise ratio was sufficiently high in the region 800-1500 *nm*.

3.4. Evaluation Methods

In this section, two evaluation methods will be described. Many variable names are used, and to avoid confusion the evaluation methods are schematically described in the Appendix by means of two flow charts.

3.4.1. Time-Resolved Evaluations

The data evaluations were based on a MATLAB program developed in-house [11]. Before the fitting procedure the instrumental response function was convoluted with the data. Here the time-resolved data was evaluated wavelength by wavelength by fitting the experimental values to the time-resolved expression for transmission using 30 mirror sources, Eqn. 2.14. The wavelength region used in the evaluations, where the signal-to-noise ratio was sufficiently high, was 800-1100 *nm*. To perform the above mentioned fit, the difference between the arithmetic expression and the time-resolved data were minimized with regards to the scattering and absorption coefficients and an amplitude factor. The minimization algorithm worked according to the Levenberg-Marquardt method, see section 2.6. The resulting scattering and absorption coefficients from this fit will hereafter be mentioned as the original scattering and absorption coefficients.

3.4.2. Method 1: Correction of NIR Data by Fixed Scattering

To mimic a simplified diode based system, five wavelength regions were selected from the recorded spectrum. However, these 10 *nm* wide regions were wider than the

bandwidth of a diode laser to compensate for the lower signal-to-noise ratio in the system used. The original scattering coefficient that corresponds to the selected wavelengths was fitted to the expression for the wavelength dependent scattering coefficient, Eqn. 2.6. The coefficients *a* and *b* were calculated and the curve was thereafter extrapolated over the wavelength range 800-1500 *nm*, which is the region where the conventional NIR data were good. This extrapolated curve will be referred to as the fixed scattering coefficients. To verify the fit of the scattering coefficient a new optimization was performed with fixed μ_s', according to the method mentioned in section 3.4.1.

The conventional NIR data was transformed from absorbance to transmission, T_{NIR}, according to Eqn. 2.16. The transmission, $T_{theoretical}$, is described by Eqn. 2.15. To minimize Eqn. 3.1 with regards to the absorption coefficient, *C* had to be determined.

Eqn. 3.1

$$T_{NIR} = C \cdot T_{theoretical}(\mu_a, \mu_s')$$

By inserting the original absorption and fixed scattering coefficients from the selected wavelength regions into the theoretical expression, *C* was found.

The fixed scattering coefficient was inserted in the theoretical expression and thereafter the minimization of Eqn. 3.1 regarding the absorption coefficients was done by means of the MATLAB function lsqnonlin, which is a Levenberg-Marquardt algorithm. This resulted in the fitted absorption coefficient for the entire conventional NIR wavelength range.

3.4.3. Method 2: Correction of NIR Data by Fixed Absorption

In the same manner as for the fixed scattering method, the same five wavelength regions were used. *C* was calculated as mentioned above, but here the original scattering coefficient was used instead. The original absorption coefficients for the selected wavelengths was fixed and thereby referred to as the fixed absorption coefficients. These coefficients were used in the theoretical expression for transmission. As in section 3.4.2 a minimization was made which gave the calculated scattering coefficients for the selected wavelengths. The coefficients *a* and *b* were again calculated by fitting the wavelength dependent scattering coefficient, Eqn. 2.6 to the calculated scattering coefficients. The curve was thereafter extrapolated over the wavelength range 800-1500 *nm*, in which the conventional NIR data was good, to obtain the fitted scattering coefficient. Hereafter the procedure to find the fitted absorption coefficients values for the entire wavelength region was the same as in Method 1.

3.4.4. Reference Analysis

In order to determine the amount of active substance in the tablets, a reference analysis was performed. The reference analysis was made by an UV/vis spectrophotometer, which is a diode array instrument. The spectral resolution was 1 *nm*. The absorption was measured at 274 *nm* and the background, measured at 550 *nm*, was subtracted. After weighing the tablets they were put in a volumetric flask with a phosphate buffer with pH 3.0. The flask was shaken mechanically for 30 minutes to dissolve the tablet.

The samples were then further diluted to volume with phosphate buffer pH 3.0 and left to sedimentate for three hours. Finally 5 ml of the clear solution were transferred to a volumetric flask of 50 ml that was filled to volume with phosphate buffer pH 3.0.

3.4.5. Multivariate Analysis

Multivariate Analysis was made to examine the ability of the methods to predict the amount of active substance in the tablets. The analysis was performed with a program called SIMCA (ver P 10.0.4.0 Umetrics, Umeå, Sweden). Regular PLS with mean centred data was used in the wavelength region 800-1350 *nm*. The number of principal components was selected to best describe the information in the data set without including noise, and the selection was mainly based on the evaluations made by SIMCA.

4. Results and Discussion

In Eqn. 2.11, and thereby in all equations containing z_e, the refractive index appears. Since this index was not determined for the pharmaceutical tablets used in this work, the index was set to 1.44 based on the determined index for microcrystalline cellulose in reference [10]. This is thought to be a good approximation, since the tablets mainly consisted of microcrystalline cellulose.

For both Method 1 and Method 2 the time dispersion curve was fitted to the time-resolved transmission, Eqn. 2.14. The fit for one wavelength is imaged in Figure 4.1 together with the instrumental response function and the measured signal. These fittings were in general successful.

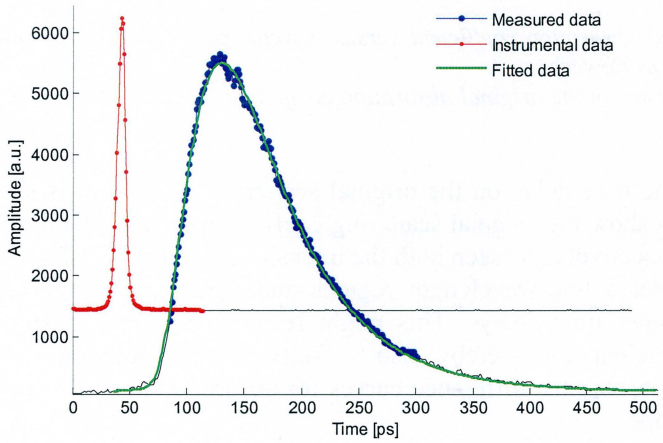

Figure 4.1
The measured and fitted time dispersion curve and instrumental function for one wavelength.

4.1. Instrumental Time Delay

The filter mentioned in section 3.2.2 implies a time delay for the instrumental function in relation to the sample measurement. Given the thickness and refractive index of the filter, 1.91 *mm* and 1.5, respectively, the time delay was calculated to 3.18 *ps*. However, this time delay resulted in negative original absorption coefficients, which made further evaluations impossible. By evaluating a number of samples with Method 1 for different time delays and estimate the performance of the absorption coefficient fit visually, the most suitable time delay was found to be approximately 35 *ps*. The same adjustment has been made by other research groups [12].

The effect on the optical properties when changing the time delay from 3.18 *ps* to 35 *ps* was studied. As seen in the left part of Figure 4.2 the original absorption coefficient is highly affected by the time delay, and is therefore no longer negative for a time delay of 35 *ps*. As seen in the right part of Figure 4.2, where the difference in the original absorption coefficient between two evaluations with different instrumental delays for the same sample is shown, it is evident that not only an offset is introduced when the time delay is increased but also a strongly wavelength dependent error.

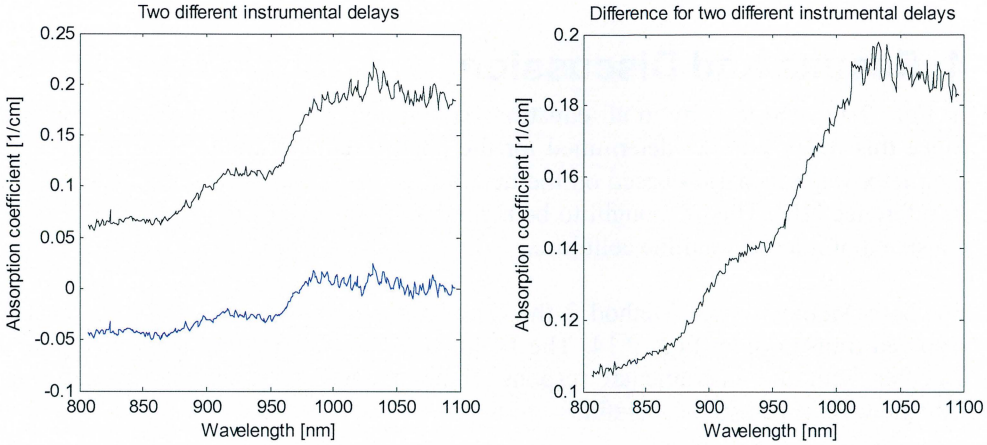

Figure 4.2
Left: The original absorption coefficient versus wavelength for the instrumental delay 35 ps (upper) and 3.18 ps (lower).
Right: The difference in the original absorption coefficient for the instrumental delays used on the left.

The effect of the time delay on the original scattering coefficient is shown in Figure 4.3. The figures show the original scattering coefficient for the actual time delay, 3.18 *ps* and 35 *ps* respectively. As seen both the intensity as well as the shape of the curve is altered. To select a few wavelength regions and obtain an appropriate fit is more difficult for higher time delays. This might result in an erroneous fit of the fixed scattering coefficient and thereby also a faulty fitted absorption coefficient. It is interesting to note that the difference curves for absorption and scattering coefficients have similar shape.

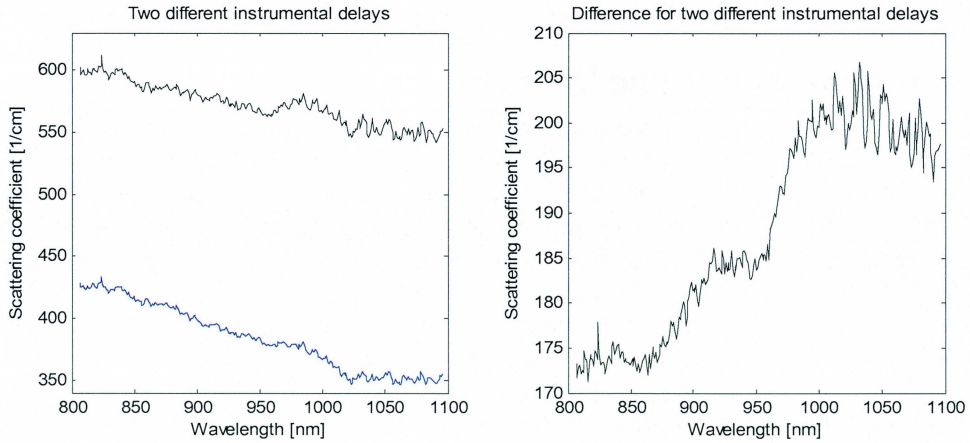

Figure 4.3
Left: The original scattering coefficient versus wavelength for the instrumental delay 35 ps (upper) and 3.18 ps (lower).
Right: The difference in original scattering coefficient for the instrumental delays used on the left.

Despite all the problems that follow this increased time delay, it was the only way to be able to perform the evaluations of interest, and therefore 35 *ps* was used in the following analysis.

4.2. Method 1: Correction of NIR Data by Fixed Scattering

Many of the original scattering coefficient plots appear noisy in the first and last part of the measured wavelength range. However, there appears to be valuable information even in the noisy signals at long wavelengths. Therefore the wavelengths for the evaluations were selected more or less evenly distributed in the following intervals: 850-859, 900-909, 950-959, 1000-1009 and 1070-1079 *nm*. In Figure 4.4 the original scattering in these intervals are encircled. The left part of the figure shows an unsuccessful fit to the original scattering coefficient, and this verifies the difficulties in selecting the appropriate wavelength regions. The wave pattern does not have the same shape for all samples, which leads to the conclusion that it is impossible to find five regions that would give a correct fit for all samples. The right part of Figure 4.4 is an example of a successful fit. Here the noise in the beginning and the end is clearly seen even though the scattering curve is smooth.

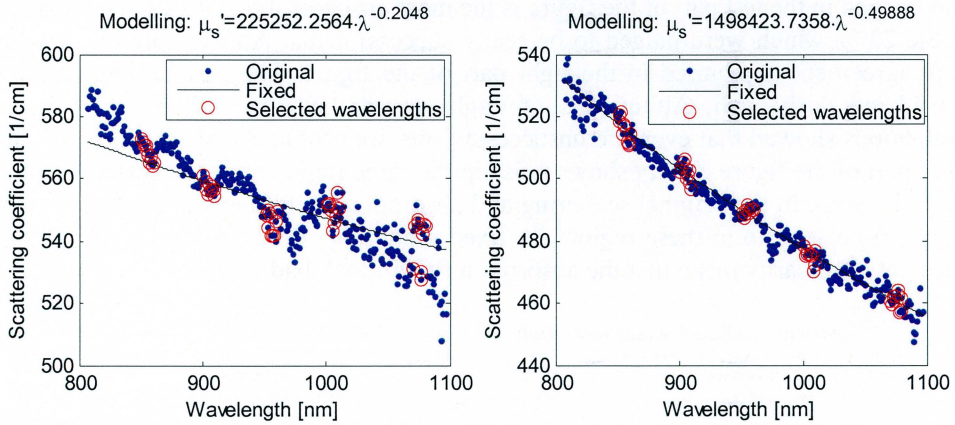

Figure 4.4
Left: Example of an unsuccessful fit to the original scattering coefficient.
Right: Example of a successful fit to the original scattering coefficient.

A typical result for the fitted absorption coefficient for the entire conventional NIR wavelength range is compared to the original absorption coefficient in the time-resolved wavelength range in Figure 4.5.

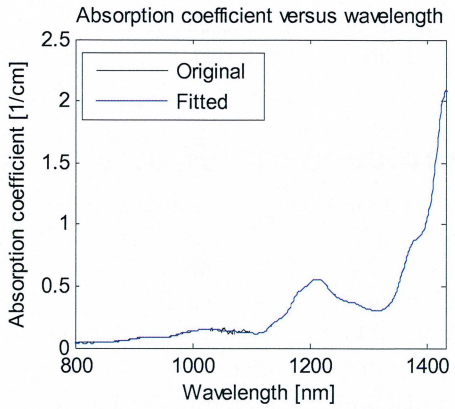

Figure 4.5
The fitted absorption coefficient for the wavelength range of interest.

Figure 4.6 shows the wavelengths overlap for the original and fitted absorption coefficient for an unsuccessful and a successful fit respectively. Based on an objective visual evaluation of the fits, barely 5 % were considered to be rather bad, where the one imaged in the left part of the figure is the most unsuccessful. This can be compared to the 23 % which were judged to be really successful fits. An example of a fit with high agreement is pictured in the right part of the figure. The maintaining fits were considered fairly well. Although a fit might appear bad, the coming chemometric evaluations showed that even the unsuccessful fits are useful, see also section 4.5. The right part of the figure clearly shows noise in the same region as in the scattering plots. Both the noise in the original scattering and absorption coefficients is due to the lower signal-to-noise ratio in these regions. A fixed scattering coefficient that is slightly off does not necessarily mean that the absorption fit will look bad.

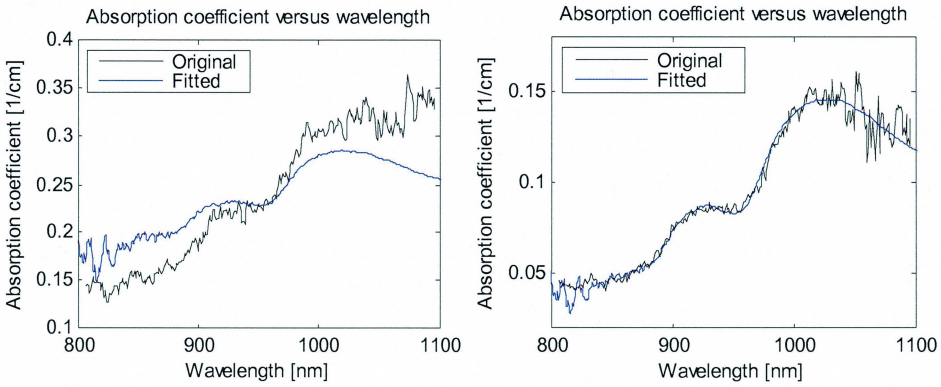

Figure 4.6
Left: The wavelengths overlap for the original and fitted absorption coefficient. An unsuccessful fit is shown.
Right: The wavelengths overlap for the original and fitted absorption coefficient. A successful fit is shown.

The main source of error could be related to the adjusted time delay that had to be used. As seen in Figure 4.2 and Figure 4.3 errors were introduced when the time delay was changed. Evidently this resulted in unknown errors in the evaluations. However,

these alterations were performed to correct for obvious errors with negative absorption coefficients. Therefore it is of greater interest to get to the bottom with why a time shift seemed necessary. Many factors might have influenced the measurements and the evaluations that lead up to the negative absorption coefficient. There might have been some systematic errors in the system. Also it can be questioned whether the tablet could be approximated with a slab or not, since there might have been effects at the boundaries that would have required a different theoretical approach. However, these considerations fall outside the scope of this thesis.

4.3. Method 2: Correction of NIR Data by Fixed Absorption

The same wavelength regions, as in Method 1, were selected to extract the fixed absorption coefficients and to calculate the corresponding scattering coefficients. These calculated scattering coefficients are encircled when imaged. Different time delays were investigated to find the best agreement with the original scattering coefficient and the fitted scattering coefficient. Due to the difficulties to find the appropriate time delay, the same delay as in Method 1 was selected. Unfortunately many fits appear to disagree totally. An example of this can be seen in the left part of Figure 4.7. The slope of the fitted scattering is here too steep, but in many cases the slope was too flat. This resulted in that there is no common time delay that gives a proper result for all samples. The amount of good fits was 23 %, the amount of fits with too flat slope was 31 % and the amount of fits with too steep slope was 46 %. The successfulness of the fits was again estimated by an objective visual evaluation. The right part of Figure 4.7 shows the absorption coefficient that corresponds to the scattering on the left. Although the fitted scattering coefficient is deviant from the original scattering coefficient, the fitted absorption is good, which is a consequence of that the evaluation is made with fixed absorption coefficients for the selected wavelengths.

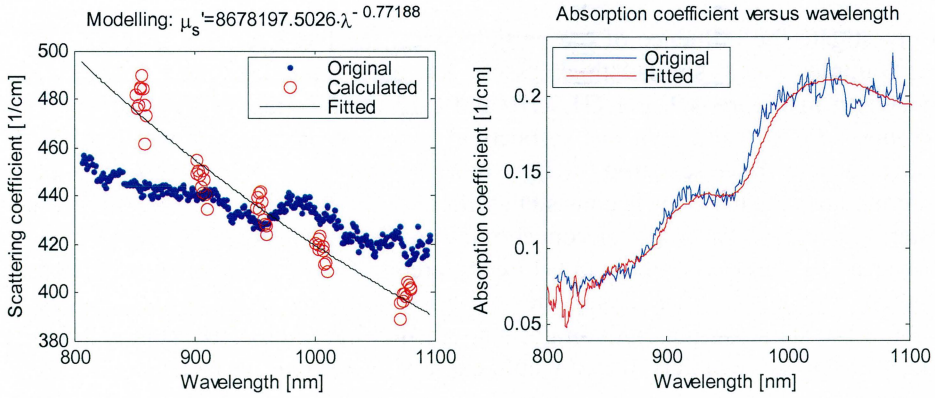

Figure 4.7
Left: Example of an unsuccessful fit to the original scattering coefficient.
Right: The original and fitted absorption coefficients corresponding to the scattering coefficient on the left.

In Figure 4.8 an example of a good agreement between the original scattering coefficient and the fitted scattering coefficient is shown. The absorption fit for the same sample is imaged in the right part of the same figure.

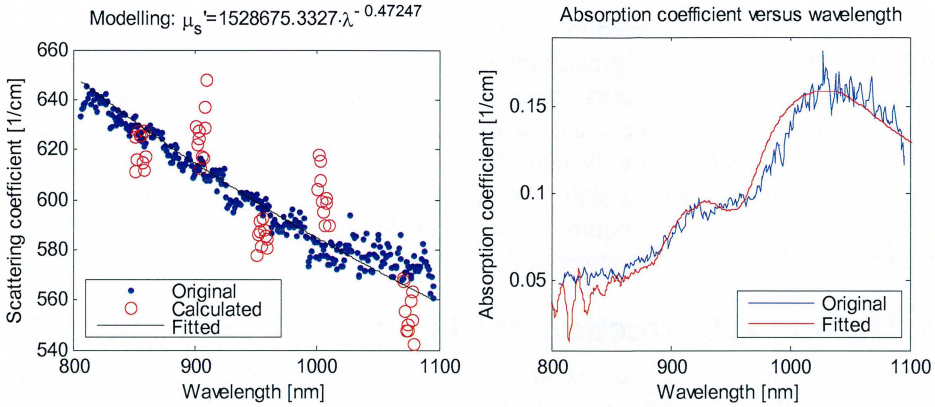

Figure 4.8
Left: Example of a successful fit to the original scattering coefficient.
Right: The original and fitted absorption coefficients corresponding to the scattering coefficient on the left.

The sources of error are in general the same as for Method 1. Whether the fitting errors occur for the same samples as in Method 1 has been investigated. The discrepancy in the fitted scattering coefficients occurs more frequently for Method 2 than the discrepancy in the fitted absorption coefficients for Method 1. The discrepancies also do not seem to appear for the same samples. However, it is hard to compare failure of the fixed scattering method and the fixed absorption method.

4.4. The Effects of Physical Properties on Scattering

It is of interest to know how the thickness, the particle size and the granulate affects the original scattering coefficient. Since these original values fluctuate, it is better to use the fixed scattering coefficients from Method 1 in this comparison.

To investigate the influence of the particle sizes, the fixed scattering coefficients for three samples, with similar thicknesses, for each granulate were plotted versus wavelength in Figure 4.9. For G1, G10 and G17 the thicknesses were approximately 2.05 *mm,* 2.06 *mm* and 1.99 *mm* respectively. The expected result would be that the smaller particles have scattered the light more and would thereby give rise to a higher scattering coefficients. This is consistent with all three granulates. It also seems like the scattering decreases with higher concentration of active substance, since the scattering is lower in G10 and even lower in G17 compared to G1. To increase the concentration of active substance, microcrystalline cellulose is replaced by active substance to maintain the same weight. This might suggest that the microcrystalline cellulose is a main scatterer in the tablets, which would explain the decreased scattering.

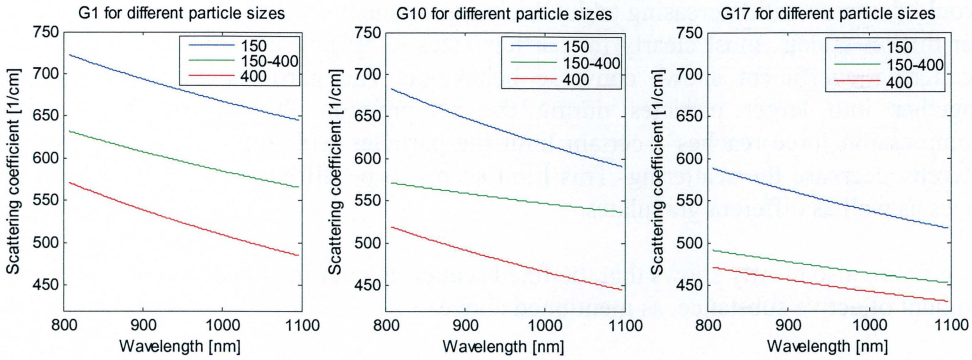

Figure 4.9
The fixed scattering coefficient versus wavelength for each granulate and different particle sizes.

To further investigate the dependency on thickness, samples with varying thickness for the different particle sizes of granulate G10 were explored. The tablet thicknesses were approximately 2.06 *mm*, 2.20 *mm* and 2.40 *mm* for the thin, intermediate and thick tablets, respectively, for all particle sizes.

Between the particles in the tablets there are small cavities of air. In thick tablets (less compressed) these cavities are larger and thereby the number of scattering events per unit length will be fewer than for a thin tablet. The most probable result would therefore be that thin tablets would scatter more than thick. Contrary to this expectation, all parts of Figure 4.10 show that the thinnest tablets scatter the least. No special order can be determined for the thick and intermediate tablets.
As mentioned in section 3.1 the only thing differing between the thicknesses is the compression force used when manufacturing the tablets. What happens with the particle sizes when the tablets are manufactured is not known, but it appears as if the particles are lumped together into larger particles. This would explain the low scattering for the thinnest samples in Figure 4.10.

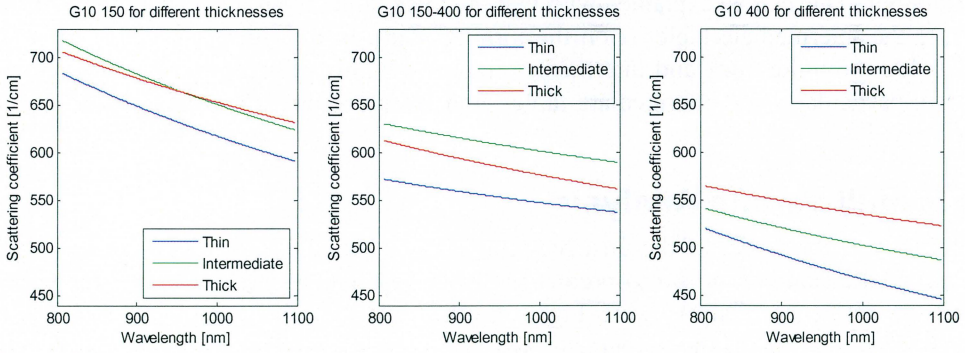

Figure 4.10
The fixed scattering coefficient for each granulate and different thicknesses.

In order to clarify the dependence on thickness the fixed scattering coefficients at one chosen wavelength for all granulates were plotted versus thickness. As seen in Figure 4.11, the scattering is highest for intermediate thicknesses and then decreases for both thicker and thinner tablets. The expected dependency would be that the scattering

would decrease with increasing tablet thickness, as mentioned above. This is seen only for thicker tablets, most clearly for particle sizes <150 μm. For thin tablets the fixed scattering coefficient shows converse behaviour. The particles may have lumped together into larger particles during the compression. It appears as when the compression force reaches a certain limit the particles will form larger particles and thereby decrease the scattering. This limit seems to be different for different particle sizes as well as different granulates.

The figure also clearly shows that the fixed scattering coefficient decreases with higher amount of active substance, as mentioned above.

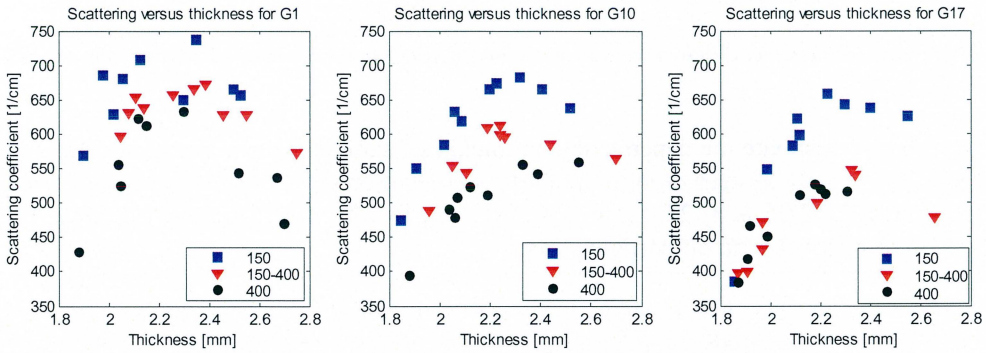

Figure 4.11
The fixed scattering coefficient versus thickness for all tablets of all granulates.

With help of the middle part of Figure 4.11, the variations in Figure 4.10 will be explained. The limit where the scattering changes appears to be around 2.30 *mm*, 2.20 *mm* and greater than 2.50 *mm* for G10 150, G10 150-400 and G10 400, respectively. The thicknesses for the intermediate and thick tablet in the left part of Figure 4.10, describing G10 150, happen to be on the plateau where the scattering dependence on thickness turns, which explains their similar scattering coefficient. In the middle part of Figure 4.10, G10 150-400, the intermediate and thick tablet shows the expected behaviour. This can be explained with that the thick tablet is far away from the plateau, while the intermediate tablet is on the turning point. In the right part of Figure 4.10, G10 400, both the thick and intermediate tablet is highly affected by the compression force, particularly the intermediate tablet, and therefore the scattering coefficient has decreased.

4.5. Multivariate Analysis

To examine the effect of the unsuccessful fits in Method 1, all fits considered good were used as calibration set to predict the bad ones. The agreement of the prediction and the reference analysis were high. Another test was made with all bad fits as calibration set. Again the agreement was high, although slightly worse than for the predictions with the good fits as calibration set. Based on these tests all samples were included in the analysis. Due to the low amount of good fits for Method 2, the same test was not performed. Therefore the evaluations were made with all samples.

The results are presented in the tables below where the preferred number of principal components is shown with bold numbers. The methods evaluated are conventional NIR

spectroscopy, fixed scattering (Method 1) and fixed absorption (Method 2). The values are given in % RMSEP.

4.5.1. Evaluation based on thickness

Table 1 presents the results when the calibration set included 31 samples and was based on all tablets thinner than 2.1 *mm*. It appears as though both the fixed scattering method and the fixed absorption method predicted the validation set with less error than conventional NIR spectroscopy. The most successful was the fixed scattering method.

Table 1
Thinner tablets than 2.1 mm (31 samples)

Principal components	NIR [% RMSEP]	Fixed scattering [% RMSEP]	Fixed absorption [% RMSEP]
5	6.18	**2.07**	**3.06**
6	**3.32**	1.91	2.23

When using all tablets thinner than 2.0 *mm* the calibration set consisted of 17 samples. Again both fixed scattering and fixed absorption are better than conventional NIR spectroscopy and fixed scattering are better than fixed absorption.

Table 2
Thinner tablets than 2.0 mm (17 samples)

Principal components	NIR [% RMSEP]	Fixed scattering [% RMSEP]	Fixed absorption [% RMSEP]
4	5.85	**2.40**	**3.68**
5	**5.22**	2.43	2.04

For tablets thicker than 2.5 *mm* (12 samples) the results from fixed scattering and fixed absorption are similar and both outdo conventional NIR spectroscopy. The fewer samples needed to predict the remaining samples, the more stable are the measurements, although when creating a stable model it is desirable to use a large set of samples. Since 12 samples of 82 are rather few, it seems like fixed scattering and fixed absorption are stable methods for this calibration set.

Table 3
Thicker tablets than 2.5 mm (12 samples).

Principal components	NIR [% RMSEP]	Fixed scattering [% RMSEP]	Fixed absorption [% RMSEP]
4	**11.20**	4.60	**3.71**
5	11.53	**3.58**	2.60

4.5.2. Evaluation based on particle size

The 27 tablets with particle sizes greater than 400 μm were used as calibration set in Table 4. Again the fixed scattering and absorption exceed conventional NIR spectroscopy. Since it is possible to choose fewer principal components for fixed

scattering and still give better results than fixed absorption, this method can be considered more stable.

Table 4
Tablets with particle sizes greater than 400 μm (27 samples).

Principal components	NIR [% RMSEP]	Fixed scattering [% RMSEP]	Fixed absorption [% RMSEP]
3	5.42	**2.76**	4.73
4	5.82	3.84	5.75
5	5.22	3.42	**3.09**
6	**5.32**	11.24	9.95

Another calibration set used every other tablet with particle size between 150-400 *μm*. The method with fixed scattering is most successful and conventional NIR spectroscopy is least successful.

Table 5
Every other tablet with particle size 150-400 μm (14 samples).

Principal components	NIR [% RMSEP]	Fixed scattering [% RMSEP]	Fixed absorption [% RMSEP]
4	**4.76**	**3.68**	**4.47**

When selecting three thin tablets from each granulate with particle size less than 150 *μm*, conventional NIR spectroscopy is the most successful predictor.

Table 6
Three thin tablets from each granulate with particle size <150 μm (9 samples)

Principal components	NIR [% RMSEP]	Fixed scattering [% RMSEP]	Fixed absorption [% RMSEP]
4	**5.68**	**7.92**	**8.34**

It is interesting to note how well fixed absorption manages to predict the amount of active substance although the fitted scattering coefficient can be totally off. But in most cases the fixed scattering method seems to be the best predictor.

5. Conclusions

Two evaluation methods were examined to separate the absorption from conventional NIR measurements by using time-resolved spectroscopy and diffusion theory. When observing the scattering coefficient received from the time-resolved measurements, conclusions about the physical parameters were made. It appeared as if the particles in the tablets were lumped together when the compression force during manufacturing reached a certain limit.

Another interesting phenomenon has been observed when comparing the scattering for tablets with different amount of active substance. The scattering decreases with increasing concentration of active substance. This suggests that the microcrystalline cellulose is a main scatterer in the tablets, and this is an additional source of error for conventional NIR spectroscopy. Other sources of error are the thickness and the particle size that also influence the scattering. Since conventional NIR spectroscopy is unable to distinguish between absorption and scattering, changes in scattering might be misread as changes in concentration of active substance.

Chemometrics showed that both evaluation methods investigated in this thesis are better to predict the amount of active substance, based on their ability to separate the absorption from the scattering which is dependent on many physical parameters. Both when the calibration set contained of a few thin or thick tablets and tablets with a certain particle size, the predictions for both methods were in general better than for conventional NIR spectroscopy. The two evaluation methods appeared more robust since they are able to predict tablets with features differing from the ones in the calibration set. The method with fixed scattering often produced the best results.

6. Future Work

It is of great importance to find the origin of the errors that causes the negative absorption coefficient. Some of the issues to analyze is the system, the evaluations and to find a good explanation for the increased time delay. The effects of the time delay adjustment influence the scattering and absorption coefficient to a great extent. To investigate whether there might have been some systematic errors in the system or the evaluations is thereby important.

Approximating the tablet shape with a slab ignores boundary effects that might influence the results. A different theoretical approach where this approximation is not done is of interest to use.

How well the evaluation methods will succeed when using a diode based laser system must be investigated.

7. Acknowledgements

First of all, we would like to thank our supervisor Christoffer Abrahamsson for always taking time to discuss with us and giving us advice. You have always been positive and in a very good mood.

We would also like to thank Stefan Andersson-Engels for his supervision and for the opportunity to write this thesis at the Lund University Medical Laser Centre.

Last but not least, we would like to thank the people at the department for raising our spirits and always making us feel welcome. Also big thanks for all the help you have given us.

8. References

[1] C. af Klinteberg, "On the use of light for the characterization and treatment of malignant tumours", Ph.D. Thesis, Lund Institute of Technology, Lund, Sweden, 1999

[2] J. Swartling, "Biomedical and atmospheric applications of optical spectroscopy in scattering media", Ph.D. Thesis, Lund Institute of Technology, Lund, Sweden, 2002

[3] S. Andersson-Engels, Lecture notes in Tissue Optics, Lund Institute of Technology, Lund, Sweden, http://kurslab.fysik.lth.se/FED4Medopt/index.htm, 2004

[4] D. Contini, F. Martelli, and G. Zaccanti, "Photon migration through a turbid slab described by a model based on diffusion approximation. I. Theory", Applied Optics, **36**, 4592-4594, 1997

[5] C. Abrahamsson, T. Svensson, S. Svanberg, and S. Andersson-Engels, "Time and wavelength resolved spectroscopy of turbid media using light continuum generated in a crystal fibre", Optics Express, **12**, 4103-4112, 2004

[6] S. Svanberg, *Atomic and Molecular Spectroscopy*, Springer, Heidelberg, 2004

[7] B. M. Wise, N. B. Gallagher, *PLS_Toolbox 2.1*, Eigenvector Research, Inc., 2000

[8] L. Eriksson, E. Johansson, N. Kettaneh-Wold, and S. Wold, *Introduction to Multi- and Megavariate Data Analysis using Projection Methods (PCA & PLS)*, Umetrics AB, 1999

[9] A. M. K. Nilsson, C. Sturesson, D. L. Liu, and S. Andersson-Engels, "Changes in spectral shape of tissue optical properties in conjunction with laser-induced thermotherapy", Applied Optics, **37**, 1256-1267, 1998

[10] M. Österberg, "On the Interactions in Cellulose Systems: Surface Forces and Adsorption", Ph.D. Thesis, Royal Institute of Technology, Stockholm, Sweden, 2000

[11] T. Svensson, Private communication, Atomic Physics Department, Lund Institute of Technology, Lund, Sweden, 2004

[12] A. Pifferi, A. Torricelli, A. Bassi, P. Taroni, and R. Cubeddu, "Performance assessment of photon migration instruments: the MedPhot protocol", (Accepted to be published in Applied Optics)

9. Appendix

Method 1:

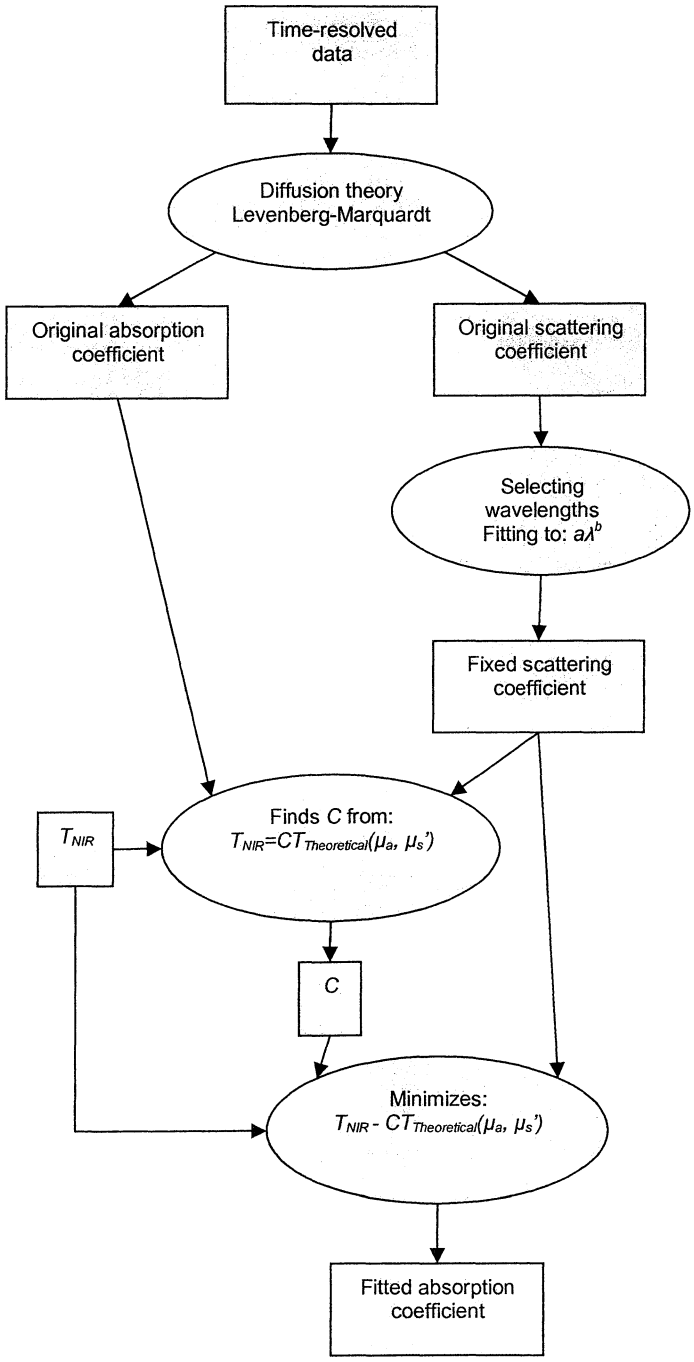

Method 2:

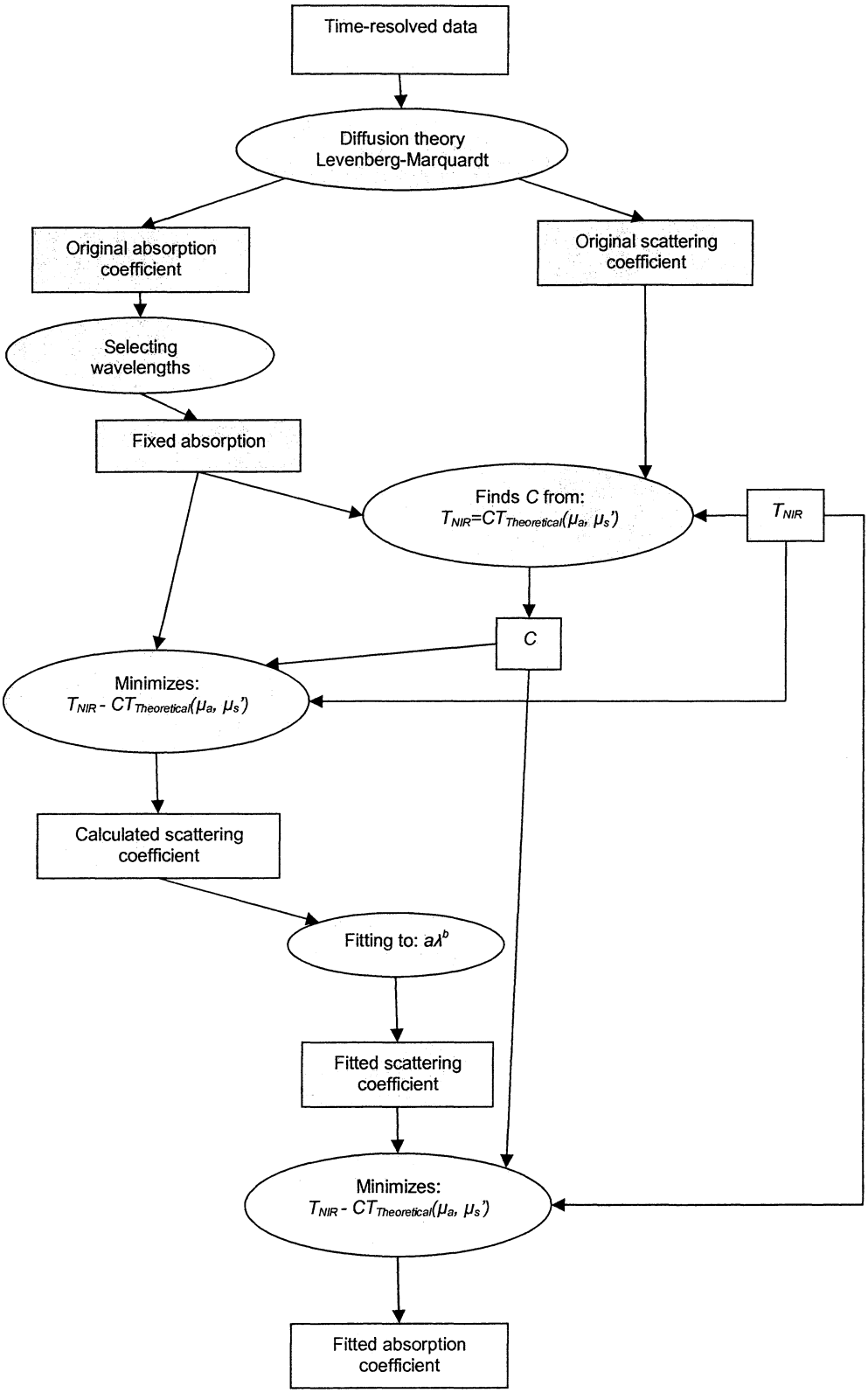
Time-resolved data
Diffusion theory
Levenberg-Marquardt
Original absorption coefficient
Original scattering coefficient
Selecting wavelengths
Fixed absorption
Finds C from:
$T_{NIR}=CT_{Theoretical}(\mu_a, \mu_s')$
T_{NIR}
C
Minimizes:
$T_{NIR} - CT_{Theoretical}(\mu_a, \mu_s')$
Calculated scattering coefficient
Fitting to: $a\lambda^b$
Fitted scattering coefficient
Minimizes:
$T_{NIR} - CT_{Theoretical}(\mu_a, \mu_s')$
Fitted absorption coefficient